Collision photography: Polarization imaging of atom-molecule collisions

R. Goldstein, C. Figl, J. Grosser, O. Hoffmann, M. Jungen, J. Stalder, and F. Rebentrost

Citation: The Journal of Chemical Physics **121**, 8769 (2004); doi: 10.1063/1.1799592
View online: http://dx.doi.org/10.1063/1.1799592
View Table of Contents: http://scitation.aip.org/content/aip/journal/jcp/121/18?ver=pdfcov
Published by the AIP Publishing

Articles you may be interested in

Absolute fragmentation cross sections in atom-molecule collisions: Scaling laws for non-statistical fragmentation of polycyclic aromatic hydrocarbon molecules
J. Chem. Phys. **140**, 224306 (2014); 10.1063/1.4881603

O-atom transport catalysis by neutral manganese oxide clusters in the gas phase: Reactions with CO, C2H4, NO2, and O2
J. Chem. Phys. **139**, 084307 (2013); 10.1063/1.4819059

Nonadiabatic electron dynamics in the exit channel of Na-molecule optical collisions
J. Chem. Phys. **128**, 224307 (2008); 10.1063/1.2928716

Nonadiabatic transitions in the exit channel of atom-molecule collisions: Fine-structure branching in Na + N 2
J. Chem. Phys. **121**, 11068 (2004); 10.1063/1.1818121

Quadrupolar spin relaxation of 14 N in NNO in collisions with various molecules
J. Chem. Phys. **109**, 10227 (1998); 10.1063/1.477718

This article is copyrighted as indicated in the article. Reuse of AIP content is subject to the terms at: http://scitation.aip.org/termsconditions. Downloaded to IP: 130.56.106.27 On: Fri, 04 Dec 2015 03:56:23

HTML ABSTRACT + LINKS

Collision photography: Polarization imaging of atom-molecule collisions

R. Goldstein, C. Figl, J. Grosser, and O. Hoffmann
Institut für Atom- und Molekülphysik, Universität Hannover, 30167 Hannover, Germany

M. Jungen and J. Stalder
Institut für Physikalische Chemie, Universität Basel, 4056 Basel, Switzerland

F. Rebentrost
Max-Planck-Institut für Quantenoptik, 85748 Garching, Germany

(Received 19 July 2004; accepted 5 August 2004)

We report differential scattering experiments on the laser excitation of $Na+M$ collision pairs with $M=N_2$, CO, C_2H_2, and CO_2. The collision event is probed by the laser polarization revealing geometric and electronic properties of the collision pair. The experimental data are compared to the results of a Monte Carlo trajectory simulation using *ab initio* quantum chemical data. © *2004 American Institute of Physics.* [DOI: 10.1063/1.1799592]

I. INTRODUCTION

The direct observation of atomic and molecular collisions is an active area of research in atomic, molecular, and chemical physics.[1,2] A considerable amount of work has been carried out on the photodissociation of weakly bound precursor molecules, a process which can also be seen as the second half of a full collision where the precursor molecule represents the transition state of the collision event.[3–6] Photoexcitation of collision pairs in real collisions has been reported for atom-atom,[7,8] atom-molecule,[9] and chemically reactive[10–12] collisions. Using crossed beams and differential detection in place of gas cell techniques, photoexcitation offers unprecedented possibilities for observing the collision event and studying the collisional interactions.[13] In particular, geometric observations of the collision complex based on polarization experiments have become possible in this way.[14,15] We study the laser excitation of atom-molecule collision pairs,

$$\mathrm{Na}(3s)+M+h\nu\rightarrow\mathrm{Na}(3p)+M,$$

in a crossed beam experiment. M is one of the linear molecules N_2, CO, CO_2, C_2H_2 in the $^1\Sigma$ ground state. The photons are detuned from the Na resonance transition and they are far from any molecular resonance. The optical excitation process is therefore restricted to configurations where the collision partners are close to each other, thus probing the collision event.

Compared to earlier preliminary experiments[16] the control of kinematic quantities has been considerably improved. Further, we are able to compare the experimental data with theoretical results, using quantum chemical data for the potential surfaces and for the electronic transition dipole moments, and a Monte Carlo trajectory approach to the collisional dynamics.

II. EXPERIMENT

The principle of the experimental setup is shown in Fig. 1. The Na atom beam, the thermal target molecule beam and two pulsed laser beams intersect each other in the scattering volume. One laser serves for the excitation of the collision pairs. The second one stabilizes the excited collision products $Na(3p)$ by transfer to a long lived Rydberg state, e.g., $Na(34d)$. The Rydberg atoms are field ionized and counted after traveling to a distant detector.

The Na atom velocities before and after the collision are determined by time of flight, using a rotating slotted disk in the Na atom beam, the timing of the laser pulses, and the arrival time of the collision products at the detector. Figure 2 shows a typical velocity distribution of the excited collision products. The symbols are the experimental points, the curve was obtained by convolution with the velocity and angular distribution functions of the beams and the acceptance function of the detector, assuming zero rotational and vibrational energy transfer. The good agreement demonstrates that the energy transfer is indeed small. The discrepancy between experiment and theory at the low velocity side might indicate energy transfer; experimental artefacts, e.g., scattering by an undirectional background target gas, are another possible origin of this structure. We used only the central part of the peak for the subsequent data evaluation.

We characterize the wavelength of the excitation laser by the detuning $(\nu-\nu_{res})/c$, where ν_{res} is the $Na(3s)\rightarrow Na(3p_{1/2})$ transition frequency. Experiments were carried out for detunings between -300 and $+480\ \mathrm{cm}^{-1}$. Laboratory scattering angles and velocities were chosen to yield center-of-mass scattering angles of 35° and a relative kinetic energy of 125 meV before the collision for all cases. In the present experiments, scattering angle and energy are not varied, rather we measure the variation of the scattered intensity with the polarization of the excitation laser. Compared to earlier similar data,[14,16] the present results are characterized by a considerably improved control of the collisional dynamics. The additional velocity selection for the Na atom beam allows a direct control of the projectile velocity, and the use of a thermal target provides a reliable control of the target velocity. As far as past and present data are comparable, there is nevertheless a reasonable agreement.

 © 2004 American Institute of Physics

This article is copyrighted as indicated in the article. Reuse of AIP content is subject to the terms at: http://scitation.aip.org/termsconditions. Downloaded to IP: 130.56.106.27 On: Fri, 04 Dec 2015 03:56:23

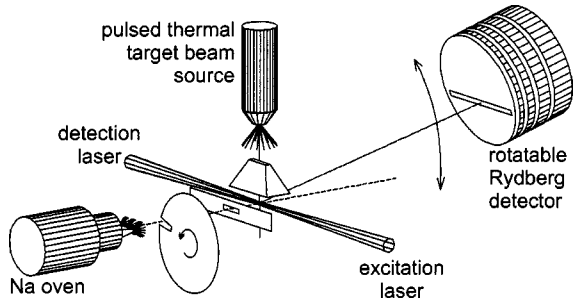

FIG. 1. The experimental setup with the crossed atomic, molecular and laser beams and the differential detector. The Na atom velocities before and after the collision are measured by the times of flight from the slotted disk to the scattering volume and from the scattering volume to the detector.

III. THEORY

A. The alignment tensor

We discuss the collision process in terms of a classical motion of the nuclei. The optical transition occurs at a nuclear configuration $\mathbf{R}_c$ where the resonance condition

$$V_f(\mathbf{R}_c) - V_i(\mathbf{R}_c) = h\nu \tag{1}$$

is fullfilled. V_i and V_f are the initial and final electronic potential surfaces of the collisional molecule. $\mathbf{R}_c$ is denoted as the Condon configuration; the transition point on the trajectory of the Na atom is the Condon point, and the vector from the center of mass of the target molecule to the Condon point is the Condon vector. Typical Na atom trajectories are shown below together with the experimental results. For a single trajectory, the dependence of the signal intensity on the polarization of the excitation laser is given by the dipole law

$$I \sim (\mathbf{E}\cdot\mathbf{d})^2, \tag{2}$$

with $\mathbf{E}$ the electric field amplitude vector and $\mathbf{d}$ the electronic transition dipole moment

$$\mathbf{d} = \langle f | e \sum \mathbf{r}_\nu | i \rangle. \tag{3}$$

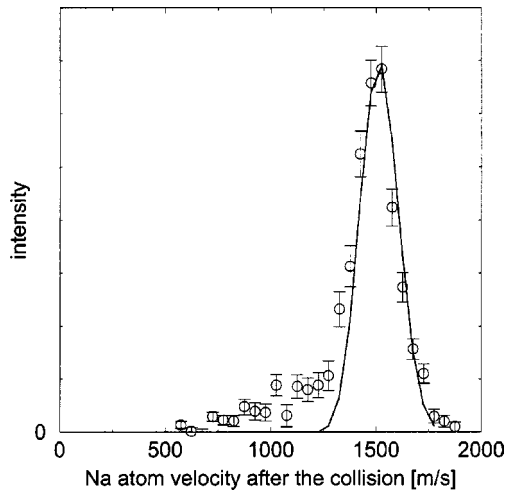

FIG. 2. Typical velocity distribution of the Na atoms after the collision. Na+CO, detuning 480 cm^{-1}.

$\langle i|$ and $\langle f|$ represent the electronic wave functions of the collisional molecule and $e\Sigma\mathbf{r}_\nu$ is the electronic dipole operator. Wave functions and transition dipole refer to the Condon configuration. In reality, many different trajectories contribute to the signal, and each trajectory has its own Condon configuration $\mathbf{R}_n$ and transition dipole $\mathbf{d}_n = \mathbf{d}(\mathbf{R}_n)$. The intensity can then be expressed as a sum

$$I \sim \Sigma p_n (\mathbf{E}\cdot\mathbf{d}_n)^2. \tag{4}$$

The p_n are weight factors for the different trajectories, see below. We consider here an incoherent superposition of the different contributions. This appears justified in view of the broad thermal distribution of the target molecule rotational states. The variation of the intensity I with the direction of $\mathbf{E}$ reflects the distribution of the transition dipole moments. When all the $\mathbf{d}_n$ have nearly the same direction in space, the intensity distribution $I(\mathbf{E})$ has a pronounced maximum when $\mathbf{E}$ points in the common direction of the dipoles and a deep minimum at right angles. When the $\mathbf{d}_n$ have a broad angular distribution, maximum and minimum become less and less pronounced. Equation (4) can be written in the form

$$I \sim \sum A_{ik} E_i E_k, \tag{5}$$

where E_j are the Cartesian components of $\mathbf{E}$. The A_{ik} form a symmetric tensor, the alignment tensor of the transition dipole moments. They are easily expressed by the p_n and $\mathbf{d}_n$. As usual, the alignment direction is defined as the direction of the largest intensity, and the contrast is $(I_{\max} - I_{\min})/(I_{\max} + I_{\min})$.

B. Electronic states

For the interpretation of the present results, we use calculations of Na+M potential energy surfaces and transition dipole moments for the lowest electronic states converging to Na atoms in the $3s$ or $3p$ states combined with ground state molecules. The molecules were kept in their equlibrium geometries in all cases, and the position of the Na atom relative to the molecular axis was varied. Details of the computational procedure are discussed elsewhere.[16–18] Cuts through the potential surfaces are shown in Fig. 3. The electronic ground state has symmetry $^2A'$, and there are three excited states, one with $^2A''$ and two with $^2A'$ symmetry.

Figure 4 shows the transition dipole moments. The target molecule is in the origin, the vector $\mathbf{d}$ is centered at the position of the Na atom. The sign of $\mathbf{d}$ is without importance in the following, $\mathbf{d}$ is therefore shown without definite direction. The $^2A' - {}^2A''$ transition dipole moments are perpendicular to the plane spanned by the nuclei, the $^2A' - {}^2A'$ dipoles are in the plane. Note that in these figures, the molecule is kept fixed whereas the Na-M axis varies. In the experiments, rather the Na-M axis is fixed to some extent and the molecular axis varies freely.

The electronic wave functions can be qualitatively characterized as a Na($3s$) orbital for the Na+M ground state and as Na($3p$) orbitals for the excited states. The alignment of the transition dipole reflects the alignment of the $3p$ orbital in the excited state. The graphs in Fig. 4 can therefore be

This article is copyrighted as indicated in the article. Reuse of AIP content is subject to the terms at: http://scitation.aip.org/termsconditions. Downloaded to IP: 130.56.106.27 On: Fri, 04 Dec 2015 03:56:23

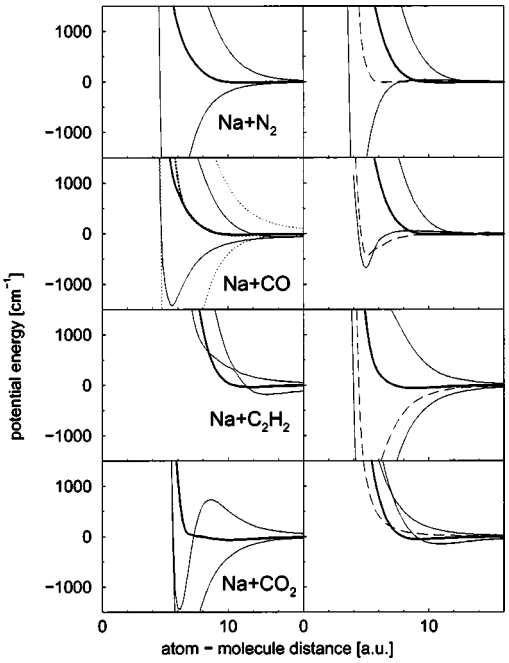

FIG. 3. Cuts through the potential surfaces. The asymptotic energies are subtracted. Left, collinear; right, *T*-shaped configurations. The X^2A' ground state potentials are shown as heavy lines, the two excited $^2A'$ potentials as light lines and the $^2A''$ potential as dashed lines; in collinear geometry, the $^2A''$ curve coincides with one of the $^2A'$ curves. For CO in the collinear arrangement, solid lines refer to the NaOC configuration, dotted lines to NaCO.

seen as maps of the excited electronic wave functions. In analogy to diatomic molecules, we speak of dipole moments with Σ character when the dipoles and hence the $3p$ orbital are close to parallel to the Na-M axis, and of Π character when the dipoles and the $3p$ orbitals are close to perpendicular to the axis. For N_2, for instance, the upper $^2A'$ state has Σ character for most of the nuclear configurations, the other two excited states rather have Π character.

The Condon configurations for different detunings are indicated as contour lines in Fig. 4. For a given detuning, only the dipole moments on the corresponding contour contribute to the process. Positive detunings probe primarily the uppermost state of $^2A'$ symmetry, negative detunings probe rather the lower excited $^2A'$ and the $^2A''$ states. Small detuning probes large atom-molecule distances, large detuning probes small distances.

C. Dynamics

We treat the collisional dynamics by a classical trajectory Monte Carlo procedure. The molecule is allowed to rotate, but the vibrational motion is frozen. The starting conditions for the orientation and rotation of the molecule are chosen at random according to a rotational temperature of 290 K. We compute the classical motion of the nuclei for a given initial relative velocity and determine the impact parameters b for which scattering to a given angle θ occurs.

For the present experiment, it is sufficient to consider trajectories leading to an azimuth scattering angle $\phi=0$, where the detector is located; such a trajecory usually starts in a plane with azimuth angle $\phi_b\neq 0$. The actual calculations are carried out with $\phi_b=0$ leading to $\phi\neq 0$. At the end the entire dataset (i.e., the Na atom trajectory, the rotating target molecule, and the transition dipole moment) is correspondingly rotated.

The Condon points are obtained according to Eq. (1) As the Condon configurations form closed surfaces (closed contour lines in Fig. 4), trajectories pass an even number of times through a Condon configuration. This leads to different

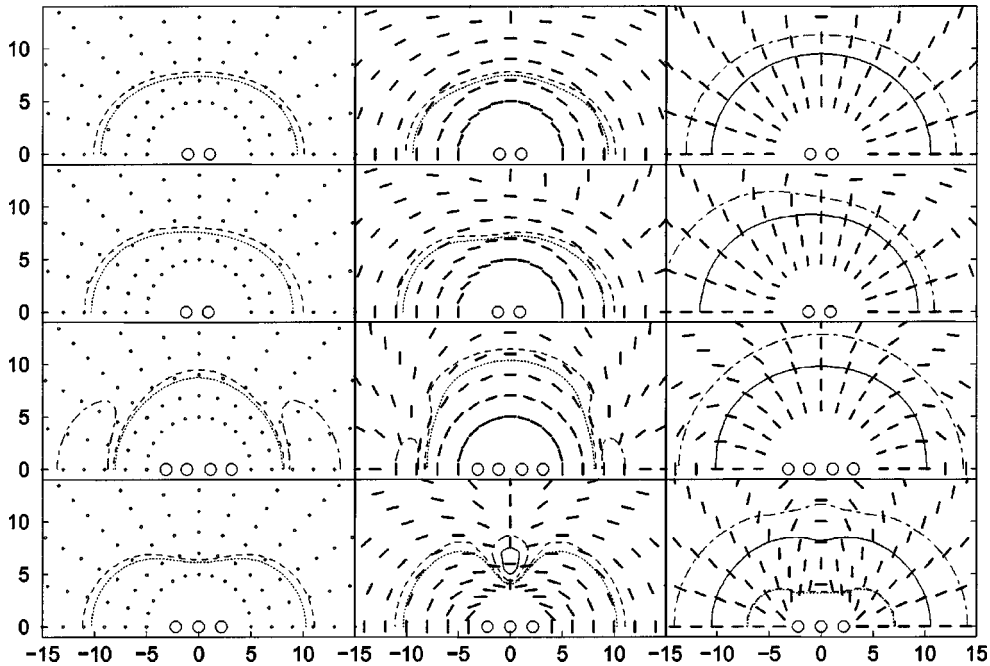

FIG. 4. The transition dipole moments between the ground state and the excited $^2A''$ (left), lower $^2A'$ (middle), and upper $^2A'$ (right) states. Top to bottom: $Na+N_2$, $Na+CO$, $Na+C_2H_2$, and $Na+CO_2$. The dipoles are shown as bars centered at the position of the Na atom. The contour lines mark the Condon configurations for the photon energies used in the experiment: solid lines 480 cm^{-1}, dot-dashed 120 cm^{-1}, dashed -182 cm^{-1}, dotted -300 cm^{-1}.

This article is copyrighted as indicated in the article. Reuse of AIP content is subject to the terms at: http://scitation.aip.org/termsconditions. Downloaded to IP: 130.56.106.27 On: Fri, 04 Dec 2015 03:56:23

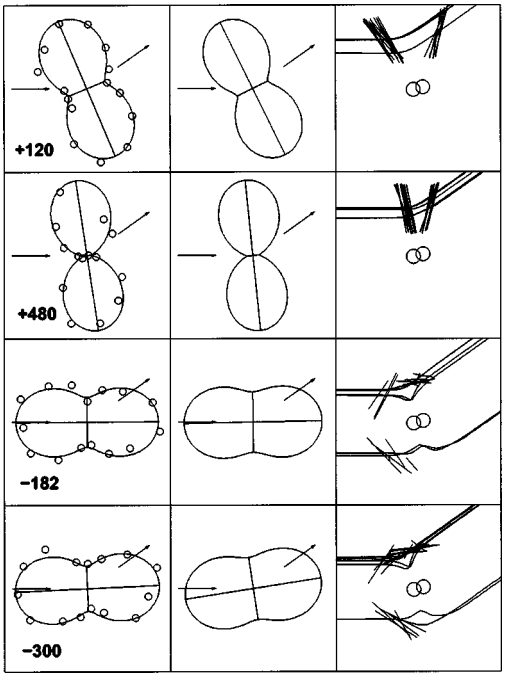

FIG. 5. Experimental and theoretical results for the optical excitation of the $Na+N_2$ collision complex. The values of the detunings are indicated in cm^{-1}. The first column shows the experimental polarization dependence of the scattered intensity in the form of a polar plot, the fit to Eq. (5) and the directions of the largest and smallest intensities. The second column gives the results calculated by the Monte Carlo trajectory approach. The arrows in the first and second columns are the relative velocity vectors before and after the collision. Sample trajectories and transition dipole vectors are shown in the third column.

types of trajectories. For type 1 trajectories, the optical transition occurs on the first passage, typically while the collision partners approach, for type 2 trajectories the transition occurs at the second passage. We further find repulsive and attractive trajectories, which are bent towards or away from the target molecule. Examples are shown in the figures below.

The transition dipole vectors $\mathbf{d}(\mathbf{R}_n)$ are computed for every Condon configuration and the weight factors are obtained as the straightforward generalization of the atom-atom case[19]

$$p_n \sim \frac{1}{|d\Delta V/dt|} \frac{b}{\sin(\theta)|\partial(\theta,\phi)/\partial(b,\phi_b)|} \tag{6}$$

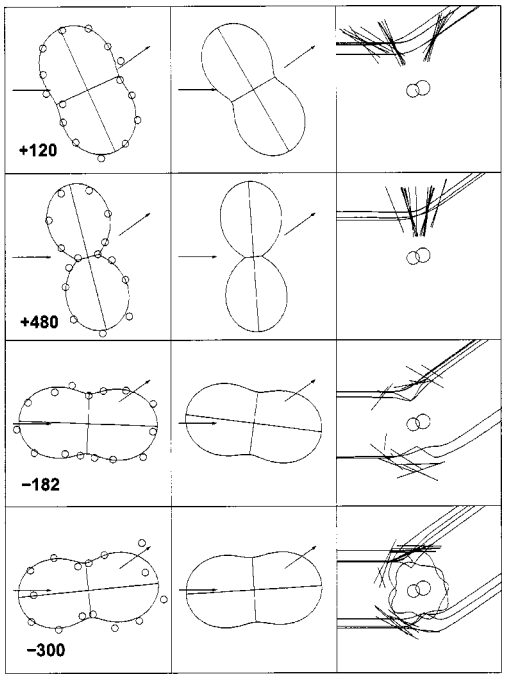

FIG. 6. Experimental and theoretical results for $Na+CO$. For details see Fig. 5.

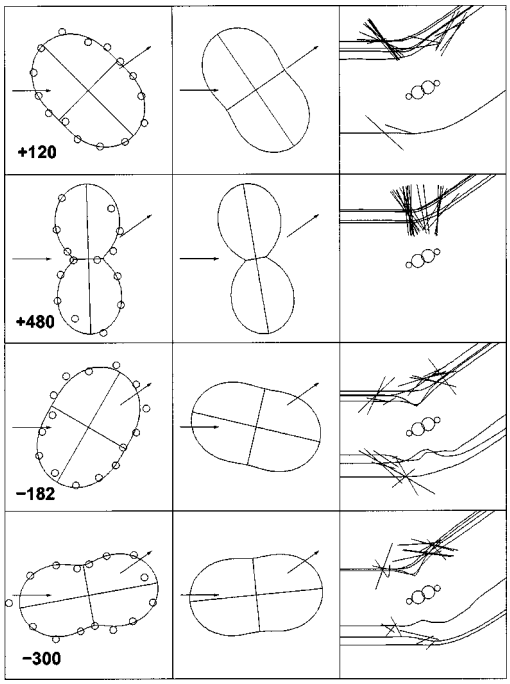

FIG. 7. Experimental and theoretical results for for $Na+C_2H_2$. For details see Fig. 5.

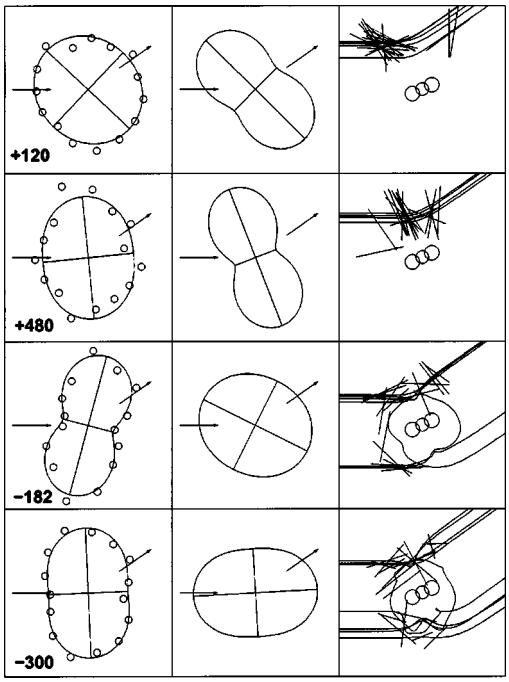

FIG. 8. Experimental and theoretical results for $Na+CO_2$. For details see Fig. 5.

This article is copyrighted as indicated in the article. Reuse of AIP content is subject to the terms at: http://scitation.aip.org/termsconditions. Downloaded to IP: 130.56.106.27 On: Fri, 04 Dec 2015 03:56:23

with $\Delta V = V_f - V_i$. The factor $|d\Delta V/dt|^{-1}$ represents the optical transition probability and can be expressed in terms of potential gradients and velocities at the Condon point. The second factor is governed by the Jacobian determinant and represents the classical scattering cross section. Exceedingly large weight factors, which are sometimes obtained with this formula are reduced using a cutoff function. The alignment tensor is obtained applying Eq. (4) to the ensemble of trajectories. We use between 500 and 1500 trajectories for this purpose. The theoretical results are finally convoluted with the angular and velocity distribution functions of the beams and the acceptance function of the detector.

IV. RESULTS

Experimental and theoretical results are collected in Figs. 5–8, where the rows correspond to detunings of 120, 480, -182, and $-300\ \mathrm{cm}^{-1}$. The first column contains the experimental data in the form of polar plots. The measured intensity is shown as a function of the laser polarization direction. The curve is a fit to the general form given by Eq. (5). The directions of the largest and smallest intensities are indicated. The data represent the projection of the alignment tensor A_{ik} on the plane scanned by the electric field vector **E**. This plane contains also the particle beam directions and the relative velocity vectors **v** and **v**′ before and after the collision. The vectors are also shown in the figures. The second column of Figs. 5–8 contains the theoretical results in the same representation. The third column illustrates the Monte Carlo simulation of the collision event showing representative selections of Na atom trajectories and transition dipole moments. Initial and final directions of the trajectories correspond to the initial and final relative velocity directions. The dipole vectors are centered at the corresponding Condon points. In most cases the Condon points form groups which represent the different types of trajectories. The group in the upper left belongs to repulsive type 1 trajectories, the group further to the right to repulsive type 2 trajectories, and the groups below the target molecule represent attractive trajectories. The number of the dipoles shown illustrates the relative weight of the different types. Note that dipole moments with Π character often form large angles with the plane of observation. As only the projection is shown, the dipoles appear shortened in this case. Every single dipole moment vector in the third column produces a contribution of the form of Eq. (2). The theoretical distributions in the second column reflect the superposition.

A. Na+N_2

Figure 5 shows a very good agreement between experiment and theory for positive detuning and a good agreement for negative detuning. The characteristic trajectories and transition dipoles in the third column should therefore provide a realistic image of the collision. At positive detuning only the uppermost repulsive $^2A'$ surface can be excited. We find therefore only repulsive type 1 and type 2 trajectories. Following Fig. 4 the transition dipole moments have Σ character throughout. Therefore, all transition dipoles are close to parallel to the Condon vector, i.e., the line from the center of the molecule to the Condon point. For $120\ \mathrm{cm}^{-1}$, the average weight of the type 1 trajectories is a factor of 3 above that of type 2. The experimental and theoretical data therefore reflect essentially the direction of the type 1 Condon vectors, the type 2 contribution is responsible for the nonzero minimum intensity. For $480\ \mathrm{cm}^{-1}$, the two groups nearly coincide, leading to a correspondingly aligned intensity distribution with a deep minimum. For negative detuning, both the lower $^2A'$ and the $^2A''$ states can be excited. The process is governed by repulsive type 1 and 2 and attractive type 1 trajectories. The intensity distribution reflects the Π character of the electronic wave functions and the preferred directions of the Condon vectors.

B. Na+CO

Figure 6 shows a good agreement between experiment and theory for positive and a very good one for negative detuning. The alignment angles for positive detuning show larger deviations than for N_2, and the comparatively low contrast of the $120\ \mathrm{cm}^{-1}$ experiment is not fully reproduced by the theory. The electronic structure, the nature of the trajectories and the distribution of the transition dipoles is quite similar as for N_2. Comparing the $120\ \mathrm{cm}^{-1}$ theoretical results for N_2 and CO, the slightly lower contrast in the second case reflects a larger scatter of the dipole directions, which is partly caused by the larger scatter of the Condon points and partly by slightly larger deviations from the predominant Σ nature of the dipoles in Fig. 4. The even lower contrast of the experimental data might indicate larger deviations from Σ character in reality. The Π type dipoles which occur just outside the $120\ \mathrm{cm}^{-1}$ Condon contour line in Fig. 4 do not contribute according to the present calculations. A small change of the transition dipole data would be sufficient to generate considerable contributions from this feature, however.

C. Na+C_2H_2

Except for $-182\ \mathrm{cm}^{-1}$, Fig. 7 shows a reasonable agreement between experiment and theory. The nature of the trajectories and the location of the Condon points is quite similar to the N_2 and CO cases according to the calculations. The low contrast in the $120\ \mathrm{cm}^{-1}$ case reflects the significant deviations from Σ character which occur in Fig. 4 for the uppermost state on the $120\ \mathrm{cm}^{-1}$ contour line. $120\ \mathrm{cm}^{-1}$ excitation can populate the other electronic states as well. The contributions are small but result in a slight further reduction of the contrast. The experimental contrast is even smaller than the theoretical result, possibly indicating even larger deviations from Σ character. The $480\ \mathrm{cm}^{-1}$ result is quite similar to those for N_2 and CO. The $-182\ \mathrm{cm}^{-1}$ data show a considerable discrepancy between experiment and theory. There is no obvious reason; for instance, a larger weight of the repulsive type 1 trajectories would bring the theory closer to the experiment. The deviations for the $480\ \mathrm{cm}^{-1}$ case are less significant, but might similarly be reduced by giving the repulsive type 1 trajectories a larger and the attractive type 1 trajectories a smaller weight.

D. Na+CO_2

For positive detuning, experiment and theory both show a low contrast. In particular, the contrast for $480\ \mathrm{cm}^{-1}$ is

This article is copyrighted as indicated in the article. Reuse of AIP content is subject to the terms at: http://scitation.aip.org/termsconditions. Downloaded to IP: 130.56.106.27 On: Fri, 04 Dec 2015 03:56:23

much lower than in the previous cases. The explanation is found in Fig. 4 where the transition dipole moments vary between Σ and Π character both on the 120 and on the 480 $\mathbf{cm^{-1}}$ contour lines, unlike in the previous cases. Again, the experimental contrast is smaller than the theoretical one. For negative detuning, a considerable discrepancy between experiment and theory is found.

V. DISCUSSION

In general, experimental and theoretical data are in good agreement. Remaining discrepancies can have their origin in the experimental procedure, in the quantum chemical data, or in the classical trajectory procedure. Two types of remaining discrepancies are encountered. For a number of cases at positive detuning (CO 120 cm^{-1}, C_2H_2 120 cm^{-1}, CO_2 120 cm^{-1} and 480 cm^{-1}), experiment and theory both show a low contrast, but the experimental contrast is still lower than the theoretical one. Experimental resolution effects are fully taken care of in the theoretical calculations and do not provide an explanation, therefore. It is tempting to ascribe the discrepancies to an underestimation of the Σ-Π variation of the transition dipoles. In three cases at negative detuning (C_2H_2, -182 cm^{-1}; CO_2, -182 cm^{-1} and -300 cm^{-1}) experimental and theoretical alignent angles deviate considerably. A trial explanation has been given for C_2H_2. It should be noted that for negative detuning, where we deal with strongly attractive surfaces, the nature of the trajectories can become complicated, with the possibility of orbiting and a rather irregular dependence of the scattering angle on the impact parameter. This sets not only limitations to our numerical accuracy but raises the question whether the classical approach and, in particular, the use of Eq. (6) and the cutoff procedure are still justified.

VI. SUMMARY

The experimental data reflect dynamical and electronic properties of the collision pair. Two quite different properties become visible. First, we see dynamical properties, like the directions of the Condon vectors and the relative weight of different types of trajectories. For instance for N_2 at a detuning of 120 cm^{-1} the measured alignment angle coincides essentially with the average Condon vector direction for the type 1 trajectories and provides a direct view of the dominant collisional geometry in this way. The nonzero minimum intensity reflects in this case the presence of a second group of Condon vectors with smaller weight. Similarly at negative detuning, where we deal with Π in place of Σ type dipoles, minimum intensity indicates the dominant Condon vector direction. Second, the data reflect the electronic structure of the collisional molecules. For instance for 120 cm^{-1}, the contrast decreases from N_2 over CO to C_2H_2 and CO_2. This reflects the different character of the transition dipoles on the 120 cm^{-1} contour line in Fig. 4. In the N_2 case, the dipoles have Σ character, independent of the relative orientation of the atom and the molecule, leading to nearly parallel dipoles in the third column in Fig. 5 and a high contrast. For CO, the deviations from Σ character are slightly larger reducing the contrast. For C_2H_2 and CO, we have contributions from Σ as well as from Π type dipoles, leading to a larger scatter of the dipole directions and to a significant reduction of the contrast.

In the C_2H_2 and CO_2 cases, the variation between Σ and Π character seems to originate from point discontinuities, where the dipoles change abruptly between Σ and Π character. These are conical intersection points, located at $r = 10.6$ a.u. at collinear geometry for C_2H_2 and at $r = 7.0$ a.u. in T-shaped geometry for CO_2; in Fig. 3, the intersections of the $^2A'$ curves in these geometries are clearly visible. For C_2H_2, strong Σ-Π variation occurs on the 120 cm^{-1} Condon contour line which lies outside the intersection point, but not on the 480 cm^{-1} line which lies inside. This results in a low contrast of the polarization data for 120 cm^{-1} and a high contrast for 480 cm^{-1}. For CO_2, both Condon curves remain outside the intersection point, resulting in a strong Σ-Π variation and a low contrast for both detunings. The present data reflect the presence and even the location of conical intersection points in this way. CO shows another related phenomenon, an apparently discontinuous change between Σ and Π character along a line. This is an avoided crossing. The feature is not reflected in the present experiments, but should become visible at smaller detuning.

ACKNOWLEDGMENTS

Financial support from the Deutsche Forschungsgemeinschaft and the Schweizerischer Nationalfond (Project No. 20-065290.01) is gratefully acknowledged.

[1] D. M. Neumark, in *Advanced Series in Physical Chemistry*, Modern Trends in Chemical Reaction Dynamics (Part 1), Vol. 14, edited by X. Yang and K. Liu (World Scientific, Singapore 2004), p. 453.
[2] P. D. Kleiber, W. C. Stwalley, and K. M. Sando, Annu. Rev. Phys. Chem. **44**, 13 (1993).
[3] A. Aguado, M. Paniagua, C. Sanz, and O. Roncero, J. Chem. Phys. **119**, 10088 (2003).
[4] A. J. Hudson, F. Y. Naumkin, O. HanBin, J. C. Polanyi, and S. A. Raspopov, Faraday Discuss. R. Soc. Chem. **118**, 191 (2001).
[5] K. Ohmori, K. Amano, H. Chiba, M. Okunishi, and Y. Sato, J. Chem. Phys. **113**, 461 (2000).
[6] S. Bililign, P. D. Kleiber, W. R. Kearney, and K. M. Sando, J. Chem. Phys. **96**, 218 (1992).
[7] W. Behmenburg, A. Makonnen, A. Kaiser *et al.*, J. Phys. B **29**, 3891 (1996).
[8] R. Goldstein, J. Grosser, O. Hoffmann, D. Wößner, G. Gerber, and H.-J. Schmidtke, Chem. Phys. Lett. **361**, 29 (2002).
[9] K. Ohmori, T. Kurosawa, H. Chiba, M. Okunishi, K. Ueda, Y. Sato, and E. E. Nikitin, J. Chem. Phys. **102**, 7341 (1995).
[10] G. A. Raiche and J. J. Belbruno, Chem. Phys. Lett. **146**, 52 (1988).
[11] M. D. Barnes, P. R. Brooks, R. F. Curl, P. W. Harlland, and B. R. Johnson, J. Chem. Phys. **96**, 3559 (1992).
[12] S. Bililign, B. C. Hattaway, T. L. Robinson, and G. Yeung, J. Chem. Phys. **114**, 7052 (2001).
[13] J. Grosser, O. Hoffmann, and F. Rebentrost, in *Atomic and Molecular Beams. The State of the Art 2000*, edited by R. Campargue (Springer, Berlin, 2001), p. 485.
[14] J. Grosser, O. Hoffmann, C. Rakete, and F. Rebentrost, J. Phys. Chem. A **101**, 7627 (1997).
[15] J. Grosser, O. Hoffmann, and F. Rebentrost, Europhys. Lett. **58**, 209 (2002).
[16] R. Goldstein, J. Grosser, O. Hoffmann, V. Schumann, D. Wößner, M. Jungen, and M. Lehner, J. Chem. Phys. **114**, 2144 (2001).
[17] M. Jungen, Helv. Chim. Acta **84**, 1459 (2001).
[18] M. Jungen, M. Lehner, R. Guérout, and J. Stalder, Phys. Chem. Chem. Phys. **6**, 1666 (2004).
[19] F. Rebentrost, S. Klose, and J. Grosser, Eur. Phys. J. D **1**, 277 (1998).

This article is copyrighted as indicated in the article. Reuse of AIP content is subject to the terms at: http://scitation.aip.org/termsconditions. Downloaded to IP: 130.56.106.27 On: Fri, 04 Dec 2015 03:56:23